

Identifying epileptogenic abnormality by decomposing intracranial EEG and MEG power spectra

Csaba Kozma^{1*}, Gabrielle Schroeder¹, Tom Owen¹, Jane de Tisi³,
Andrew W. McEvoy³, Anna Miserocchi³, John Duncan³,
Yujiang Wang^{1,2,3}, Peter N. Taylor^{1,2,3}

October 11, 2023

1. CNNP Lab (www.cnnp-lab.com), Interdisciplinary Computing and Complex BioSystems Group, School of Computing, Newcastle University, Newcastle upon Tyne, United Kingdom
2. Faculty of Medical Sciences, Newcastle University, Newcastle upon Tyne, United Kingdom
3. UCL Queen Square Institute of Neurology, Queen Square, London, United Kingdom

* c.a.kozma2@newcastle.ac.uk

HIGHLIGHTS:

- Interictal EEG biomarkers using normative maps of power in different frequencies allow us to identify epileptic abnormalities and distinguish patient outcome.
- Decomposing brain activity into periodic (oscillatory) and aperiodic (trend across all frequencies) activity may identify underlying drivers of epileptic abnormalities.
- Our findings suggest that sparing abnormalities in either periodic or aperiodic activity may lead to a poor surgical outcome, henceforth both are necessary.

KEYWORDS: Normative mapping, iEEG, MEG, Power spectrum decomposition, 1/f exponent, Epilepsy

1 Abstract

Background

Identifying abnormal electroencephalographic activity is crucial in diagnosis and treatment of epilepsy. Recent studies showed that decomposing brain activity into periodic (oscillatory) and aperiodic (trend across all frequencies) components may illuminate drivers of changes in spectral activity.

Methods

Using iEEG data from 234 subjects, we constructed a normative map and compared this with a separate cohort of 63 patients with refractory focal epilepsy being considered for neurosurgery. The normative map was computed using three approaches: (i) relative complete band power, (ii) relative band power with the aperiodic component removed (iii) the aperiodic exponent. Corresponding abnormalities were also calculated for each approach in the separate patient cohort. We investigated the spatial profiles of the three approaches, assessed their localizing ability, and replicated our findings in a separate modality using MEG.

Results

The normative maps of relative complete band power and relative periodic band power had similar spatial profiles. In the aperiodic normative map, exponent values were highest in the temporal lobe. Abnormality estimated through the complete band power robustly distinguished between good and bad outcome patients. Neither periodic band power nor aperiodic exponent abnormalities distinguished seizure outcome groups. Combining periodic and aperiodic abnormalities improved performance, similar to the complete band power approach (iEEG AUC=0.64, $p=0.05$; MEG AUC=0.69, $p=0.039$).

Conclusions

Our findings suggest that sparing cerebral tissue that generates abnormalities in either periodic or aperiodic activity may lead to a poor surgical outcome. Both periodic and aperiodic abnormalities are necessary to distinguish patient outcomes, with neither sufficient in isolation. Future studies could investigate whether periodic or aperiodic abnormalities are affected by the cerebral location or pathology.

2 Introduction

Improved EEG biomarkers of the epileptogenic zone are important, as around half of individuals have recurrent seizures after surgical treatment (de Tisi et al., 2011; Téllez-Zenteno et al., 2005; Wiebe et al., 2001). Substantial research has focused on interictal EEG biomarkers using normative maps of power in different frequencies (Bernabei et al., 2022; Frauscher et al., 2018; Taylor et al., 2022). This approach involves outlining the spatial characteristics and ranges of the feature of interest in a healthy context and comparing patient data to identify abnormalities. The invasive nature of intracranial EEG (iEEG) means that obtaining data from healthy individuals for comparison is not possible. Recent studies proposed using patient iEEG data from regions outside the epileptogenic zone to create normative maps (Betz et al., 2019; Frauscher et al., 2018; Groppe et al., 2013). The band power of different frequency bands can be used to infer expected healthy spatial profiles of EEG activity. This approach showed promising results to identify abnormalities and classify patient outcomes across different modalities (Bernabei et al., 2022; Owen et al., 2023; Taylor et al., 2022).

It is unclear what spectral features drive the observed band power abnormalities. One way to explore these features is to decompose the power spectra into rhythmic (periodic) and non-rhythmic (aperiodic) components (Buzsáki et al., 2012; Gerster et al., 2022; He, 2014; Miller et al., 2009). The aperiodic component can be described by its offset and exponent (Buzsáki et al., 2012; Miller et al., 2009), while periodic components form peaks in the power spectra. Both components should be considered, as power changes observed in specific frequency bands can be attributed to either changes in the peak or the offset (Donoghue et al., 2020a, 2022; Gao et al., 2017; Gerster et al., 2022).

Recent empirical studies have related periodic and aperiodic components to behavioral and demographic variables. There is an association between aperiodic activity and age (Donoghue et al., 2020a; Voytek and Knight, 2015; Voytek et al., 2015). Aperiodic activity varies across neural-development and decline (Ostlund et al., 2022; Tran et al., 2020) as well as in sleep (Lendner et al., 2020) and anesthesia (Colombo et al., 2019). Despite the growing interest in decomposing power spectra (Donoghue et al., 2020b; Gerster et al., 2022; Ostlund et al., 2022; Wilson et al., 2022), previous studies have not investigated which power spectrum components contribute to abnormal interictal brain activity.

Here we investigate if interictal abnormality is driven by periodic components, aperiodic components, or a combination of both components. We first present normative maps of complete band power, periodic band power, and the aperiodic exponent obtained from interictal intracranial EEG (iEEG) recordings from 234 participants. Subsequently, we identify abnormalities in spared and resected regions using recordings obtained from 63 patients with focal epilepsy. Lastly, we replicate our analysis using resting-state magnetoencephalography (MEG) recordings from 70 healthy controls and 33 patients. Ultimately, we aim to clarify if periodic and/or aperiodic abnormalities explain overall band power abnormality, and if they are both necessary to distinguish patient outcomes.

3 Methods

3.1 Patients & controls

3.1.1 iEEG cohorts

We generated normative maps using data from 234 controls from the Restoring Active Memory (RAM) data set (RAM., 2018). The second cohort was from 63 patients with refractory focal epilepsy treated at National Hospital for Neurology and Neurosurgery (NHNN) (Table 1). Surgical outcomes of seizure freedom for the UCLH cohort were assessed using the International League Against Epilepsy (ILAE) surgical outcome classification, focusing on the 12-month post-surgery period. The NHNN cohort consisted of 34 $ILAE_{1,2}$ and 29 $ILAE_{3+}$ patients, as described previously (Taylor et al., 2022).

Table 1: Summary of iEEG cohort data

	$ILAE_{1,2}$	$ILAE_{3+}$	Test statistic
n%	34 (54)	29 (46)	
Age, mean (SD)	32.3 (10.7)	33 (8.8)	p = 0.801, t = -0.252
Sex, male:female	16:18	17:12	p=0.361, $X_2=0.838$
Temporal, extratemporal	22, 12	15, 14	p=0.296, $X_2 = 1.088$
Resection hemisphere, left/right	19/15	16/13	p= 0.955, $X_2 = 0.003$
Number of electrode contacts, mean (SD)	67.5 (29.27)	65.9 (23.3)	p= 0.459, t= -0.103

3.1.2 MEG cohorts

We conducted the same analysis on magnetoencephalography (MEG) recordings using healthy controls and patients. Both groups underwent eyes-closed awake resting-state MEG using a 275-channel CTF whole head MEG system in a magnetically shielded room. Healthy control data were collected at CUBRIC, Cardiff, consists of 70 participants. Data from 33 patients with refractory neocortical epilepsy were collected at NHNN (Table 2). This patient cohort consisted of 12 $ILAE_{1,2}$ and 21 $ILAE_{3+}$ patients, as described previously (Owen et al., 2023).

Table 2: Summary of MEG cohort data

	$ILAE_1$	$ILAE_{2+}$	Test statistic
n%	12 (36)	21 (64)	
Age, mean (SD)	32.3 (10.7)	32.3 (11.3)	p = 0.058, t = 2.003
Sex, male:female	7:5	10:11	p=0.554, $X_2=0.351$
Resection hemisphere, left/right	6/6	12/9	p= 0.692, $X_2 = 0.157$

3.2 MRI processing

Pre-operative 3D T1-weighted MRI images were acquired using a 3T GE Signa HDx scanner using previously described acquisition sequences (Taylor et al., 2018). These MRI data were used to segment and parcellate different brain regions using the FreeSurfer ‘recon-all’ pipeline (Fischl, 2012). For consistency between subsequent iEEG and MEG analyses, we used a common Lausanne parcellation with 114 neocortical brain regions (Hagmann et al., 2008). For iEEG analyses we also included 14 deep brain regions including hippocampus, amygdala, thalamus, putamen and caudate. All time series analysis was performed at a brain region level, rather than at a iEEG electrode contact or MEG sensor level.

For iEEG data, we localized electrode contacts to the nearest brain regions, based on the Euclidean distance. Electrode contacts further than 5mm from a region, or located within white matter and more than 2mm from grey matter were excluded, as previously (Taylor et al., 2022).

For MEG data, we applied the minimum norm estimate technique, sLORETA, in conjunction with an overlapping spheres head model, to perform source localization, projecting onto the cortical surface (Tenney et al., 2020). This process yielded 15,000 sources that were constrained in a direction perpendicular to the cortex. Sources were downsampled into scout regions of interest, using Lausanne parcellation.

To generate resection masks we registered the postoperative T1-weighted scan to the preoperative scan using linear registration. The resected tissue was manually delineated with FSL software (Jenkinson et al., 2012), accounting for anatomical information (e.g. due to post-operative brain shift into the resection cavity). Electrode contacts within a 5mm proximity to the resection were labeled as resected. Regions were classified as resected if the volumetric change between the pre- and postsurgical measurements exceeded 25%.

3.3 iEEG processing

We used the same data as (Taylor et al., 2022) and followed those preprocessing steps. The RAM and UCLH data were downsampled to 200 Hz and a common average reference was then applied to all recordings. For the RAM cohort, channels in seizure onset zones (SOZ), early propagation zones, brain lesions, or white matter were removed, resulting in 21,598 channels across 234 participants. For the UCLH cohort, we retrospectively extracted 70 seconds of interictal iEEG recordings at least 2 hours away from any seizures. Grey matter channels without recording artifacts were included, resulting in 4,273 channels across 63 patients.

3.4 MEG processing

We used eyes-closed, awake resting state MEG preprocessed data (Owen et al., 2023). In brief, raw MEG recordings were preprocessed using Brainstorm (Tadel et al., 2011). MEG sensor locations and structural MRI scans were aligned and registered using fiducial points. The recordings were down sampled to 600 Hz and bandpass filtered from 1 to 100 Hz. Cardiac and ocular artifacts were removed using independent component analysis (ICA). Subsequently, the sources were downsampled into neocortical ROIs, using the Lausanne parcellation. We excluded deep brain subcortical regions as it is challenging to determine the neural activity or sources within the brain that give rise to the measured magnetic fields outside the head, especially for interictal recordings expected to be of low amplitude (Ahlfors et al., 2010; Baillet et al., 2001).

3.5 Estimating power spectra

Based on the preprocessed iEEG and MEG time-series data we estimated the complete power spectrum in each 70 second epoch. Using Welch’s method, we divided the time-series data into 2-second temporal windows with 1-second overlap, applied a Hamming window to each temporal window, and computed the Fourier transform, and then averaged the resulting spectra.

3.6 Decomposing power spectra

To decompose the iEEG and MEG power spectra, we used the `specparam` package (Donoghue et al., 2020a). The algorithm was used with configurations of ‘peak width limits’ = [1,8], ‘maximum number peaks’ = 6, ‘min peak height’ = 0.1, ‘peak threshold’ = 0.1, ‘aperiodic mode’ = ‘fixed’, and ‘frequency range’ = [1,30] Hz. We only used the 1-30 Hz frequency range to exclude issues with line noise and possible errors in curve fitting in higher frequencies. The decomposition sequentially fit aperiodic and periodic components to the neural power spectrum. First, `specparam` performed a robust linear fit of the spectrum to estimate the aperiodic signal (Fig. 1A) (Donoghue et al., 2020a, 2022; Gerster et al., 2022). The fitted curve was then subtracted from the original spectrum, resulting in a flattened spectrum representing periodic activity (Fig. 1A). A relative threshold was calculated based on the standard deviation of the flattened spectrum. Peaks exceeding predefined thresholds were identified iteratively, and Gaussian functions were fitted to these peaks. The fitted Gaussian curves were subtracted from the spectrum. The oscillatory components were obtained by fitting a multivariate Gaussian to all the extracted peaks simultaneously. Finally, the initial fit is added back to the flattened spectrum, resulting in the periodic component. In addition to analyzing the entire power spectrum, we focused on two specific decomposed features: periodic activity and aperiodic exponent. We calculated the complete band power and periodic band power within four frequency bands of interest (δ 1–4 Hz, θ 4–8 Hz, α 8–13 Hz, and β 13–30 Hz). The complete and periodic band power values were then \log_{10} transformed and normalized, ensuring that the sum of the band power in each contact (for iEEG data)

or ROI (MEG data) equaled one (Fig. 1, side views of the maps in Fig S1.1). In addition, we extracted aperiodic exponent values. These steps yielded the relative complete band power, relative periodic band power, and aperiodic exponent values for each subject in each of the subject's contacts (iEEG) or ROIs (MEG).

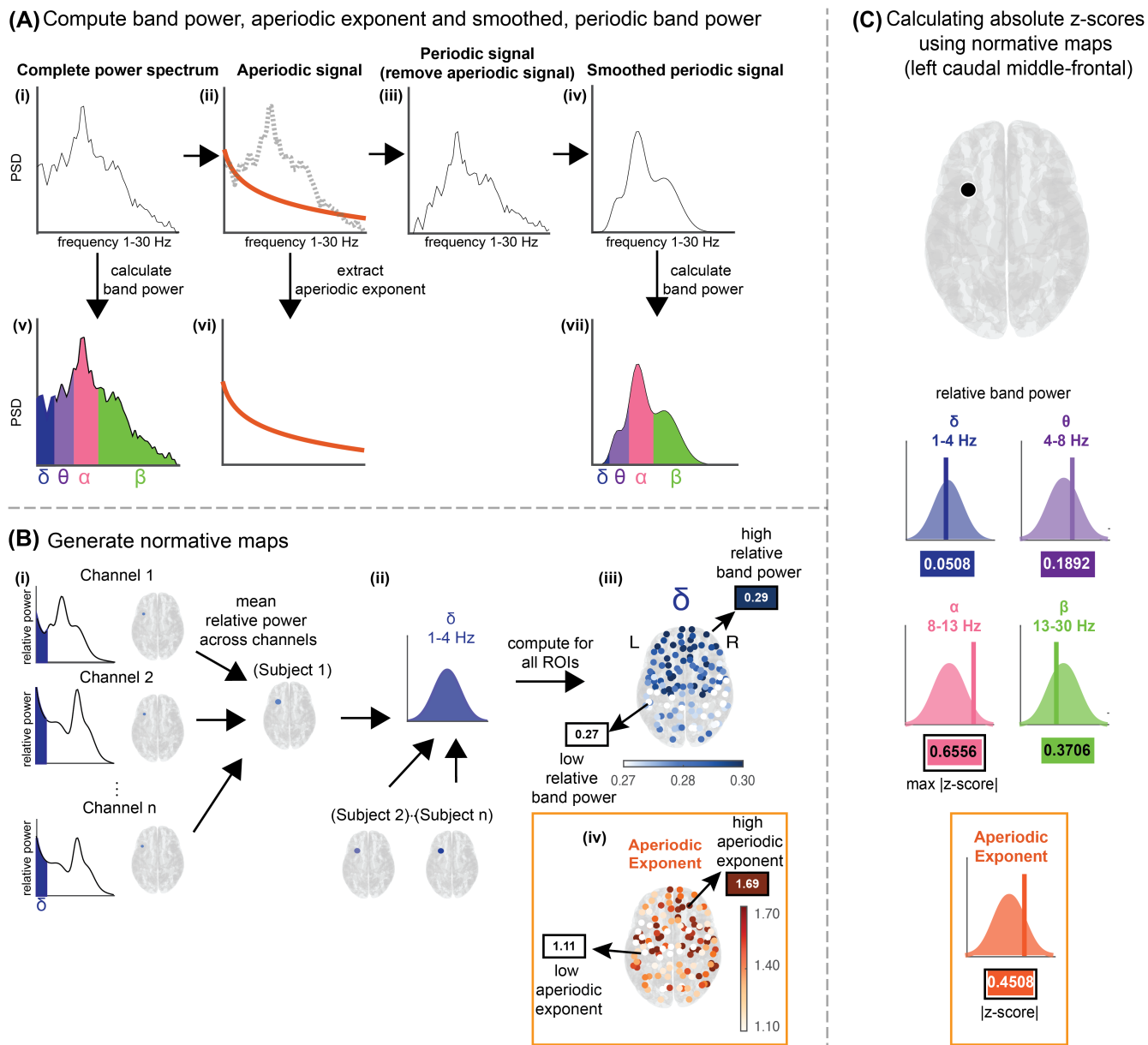


Figure 1: Computing abnormalities based on the decomposed power spectrum. (A) Decomposition of iEEG and MEG power spectra using specparam to compute relative complete band power, the aperiodic exponent, and relative periodic band power. (i) Complete power spectrum between 1-30 Hz. The power spectrum (ii, dotted grey line) was decomposed into a periodic component (iii, orange line) and aperiodic signal (iv, Smoothed periodic signal). (v) Complete band power was calculated for four frequency bands (δ 1-4 Hz, θ 4-8 Hz, α 8-13 Hz, and β 13-30 Hz). (vi) Aperiodic exponent values were extracted (orange line). (vii) Periodic band power was calculated for four frequency bands. (B) Using δ band as example to show how normative maps are generated. (i) Mean relative complete band power/relative periodic band power/aperiodic exponent were computed across contacts to get a single series of values per ROI (δ band as example). We then computed the measures for every ROI (ii) across normative map subjects. (iii) We generated the normative map, which is the spatial distribution of relative complete band power/relative periodic band power across the whole brain. (iv) We generated aperiodic exponent maps. (C) Absolute z-scores calculated across the frequency bands and the maximum was taken for every ROI, which serves as the value of abnormality.

3.7 Generate normative maps

iEEG normative maps of relative log band power values were generated for the complete power spectrum and the periodic activity. We averaged this measure across electrodes within subjects first, then across subjects within each region to compute the mean (μ) and standard deviation (σ) across subjects (eq. 1). For the aperiodic exponent values, we calculated the mean and standard deviation of exponent values across electrodes and patients within each region (Fig. 1B and Fig. 2). MEG normative maps were generated via the same method as described above and can be found in the supplementary material (Fig. S1.2).

3.8 Calculate abnormalities using normative maps

To assess the abnormality of a region’s relative band power in a patient, relative to the normative map, we calculated the absolute z-score of each region i in each frequency band j (see also Fig. 1):

$$|z_{ij}| = \left| \frac{x_{ij} - \mu_{ij}}{\sigma_{ij}} \right| \quad (1)$$

Here x represents the regional band power value for an individual patient and μ and σ the mean and standard deviations of the regional band power in the normative map. Meanwhile, i represents the region, and j the frequency band of interest. We used the maximum absolute z-score across frequency bands to define abnormality at the regional level, considering individual differences in frequency bands both in complete band power and periodic band power (Fig. 1C). Regarding aperiodic exponent, we calculated the absolute z-score of each region in the patient data set relative to the normative map.

To compare the values between resected and spared regions, we used the distinguishability statistic (D_{RS}) for each patient in the data set and frequency band (Bernabei et al., 2022; Ramaraju et al., 2020; Wang et al., 2020). The D_{RS} value indicates the abnormality difference between resected and spared regions: a value above 0.5 indicates that spared regions had higher abnormality than resected regions, while a value below 0.5 indicates the opposite. D_{RS} is equivalent to the area under receiver operating curve.

3.9 Ethics approval

The analysis of this data set was approved by the Newcastle University Ethics Committee (ref. 12721/2018).

3.10 Code and data availability

Code to reproduce figures in the manuscript will be made available upon acceptance of the paper. Deidentified PSD data will also be made available upon acceptance of the paper.

4 Results

We decomposed the power spectrum into its periodic and aperiodic components to investigate these components as potential driving mechanisms of band power abnormalities in the complete power spectrum. First, we show the normative maps of (i) complete band power, (ii) periodic band power, and (iii) the aperiodic exponent using interictal intracranial EEG (iEEG) recordings from 234 subjects. Second, we compared the abnormalities of spared and resected regions in two example patients across the three approaches. We used the D_{RS} metric to quantify the relationship between spared and resected abnormalities. Third, we compared the D_{RS} values computed from the abnormalities calculated from complete band power, periodic band power, and aperiodic exponent in interictal iEEG recordings acquired from 63 patients with focal epilepsy. Finally, we repeated our analysis using resting-state MEG recordings.

4.1 Normative maps of complete band power, periodic band power, and aperiodic exponent

We first show the spatial distribution of healthy neural activity based on complete and the decomposed spectral features. Figure 2A presents normative maps of the relative complete band power in four distinct frequency bands (δ 1–4 Hz, θ 4–8 Hz, α 8–13 Hz, and β 13–30 Hz). We then generated normative maps based on relative periodic band power, with the aperiodic component removed (Fig. 2B). These maps reveal several discernible patterns. Notably, the anterior temporal and frontal regions have the highest relative power in the delta frequency band, whereas the parietal and occipital regions show prominent relative power in the alpha frequency band. Thus, periodic band power reproduces the previously observed spatial patterns in complete band power. Figure 2C shows that the normative maps of aperiodic exponent values also have a specific spatial pattern; namely, higher aperiodic exponent values can be found in the temporal lobe compared to the rest of the brain. These results are replicated using MEG data in Supplementary Section/Figure S2.

(A) Complete band power (B) Periodic band power (C) Aperiodic exponent

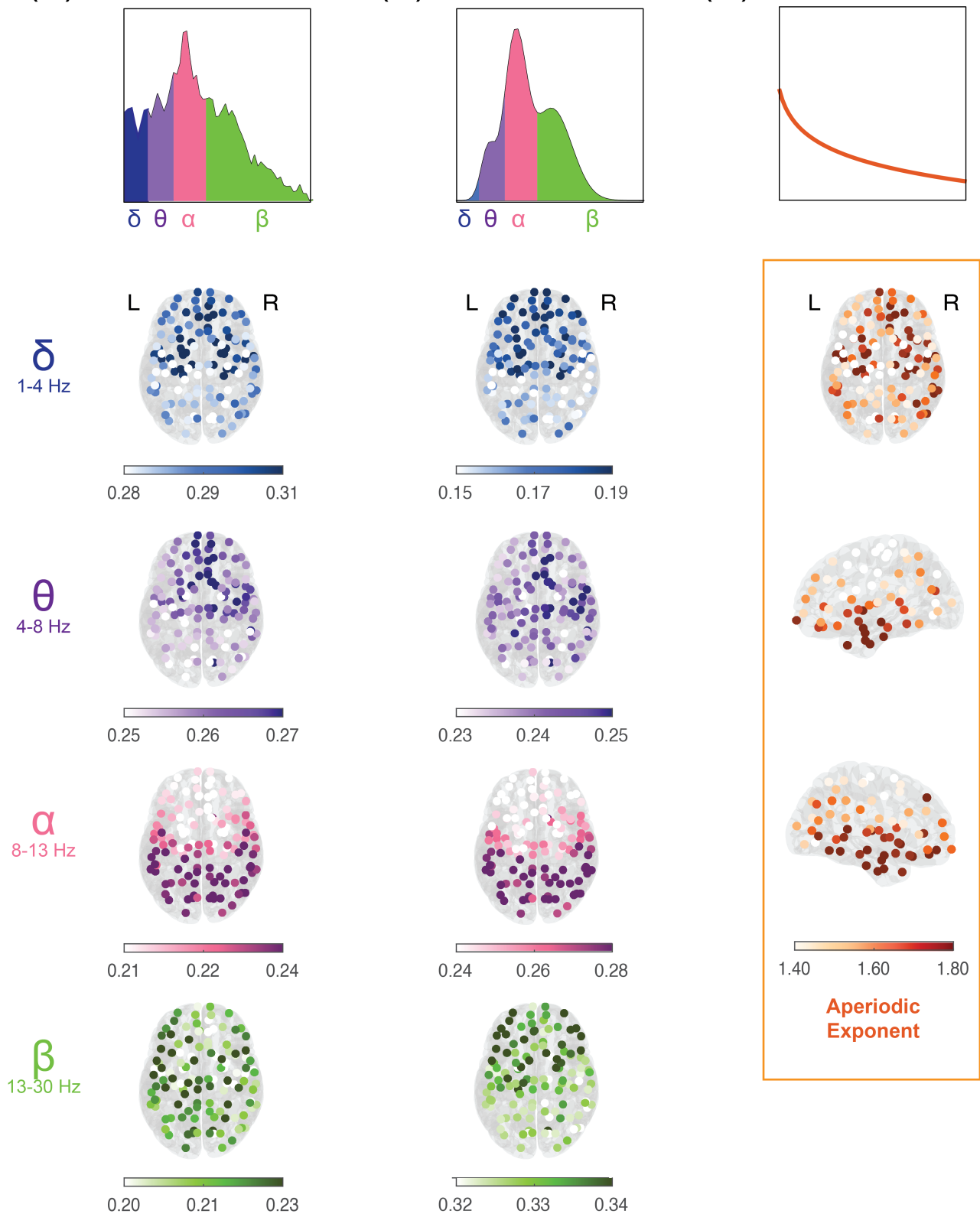


Figure 2: Normative maps of iEEG relative complete band power, relative periodic band power, and aperiodic component. Spatial distribution of mean ROI values of, (A) relative complete band power, (B) relative periodic band power, and (C) aperiodic exponent. The colour axes scale differs for each frequency band and the distribution of exponent values. Top row shows the schematic representation of each of the approaches.

4.2 Different complete band power components contribute to abnormality in different patients

We computed abnormalities in complete band power, periodic band power, and the aperiodic exponent in two example patients (Fig. 3). The abnormalities capture the largest deviation of the spectral measure from the normative distribution in each region of interest (ROI). In addition, we computed D_{RS} , the distinguishability of resected vs. spared tissue, from each type of abnormality. Figure 3A shows the abnormalities of an example patient who was seizure free after surgical intervention (ILAE 1). Both complete band power and periodic band power abnormalities yielded D_{RS} values well below 0.5 ($D_{RS}=0.14$, $D_{RS}=0.26$) and were strongly correlated in this patient (Spearman's correlation=0.90, Figure 3C). However, the aperiodic exponent abnormalities gave D_{RS} value close to 0.5 ($D_{RS}=0.44$), and were not informative for outcome nor correlated to our original measure (Spearman's correlation=0.29). Thus, the complete band power gained from the periodic signal performed better than the aperiodic exponent.

In contrast Patient 2 had poor outcome after surgery (ILAE 4)(Figure 3B). Both complete band power and aperiodic component abnormalities yielded D_{RS} values above 0.5 ($D_{RS}=0.94$, $D_{RS}=0.84$), and these abnormalities were strongly correlated (Spearman's correlation=0.72, Figure 3D). However, the periodic band power abnormalities gave D_{RS} value close to 0.5 ($D_{RS}=0.55$) and indicating similar abnormalities in spared and resected ROIs (Spearman's correlation=0.23). The aperiodic exponent solution best estimated abnormalities and patient outcome for Patient 2. Therefore, the type of component that appeared more informative about the location of abnormality and outcome of patient differed between these two patients.

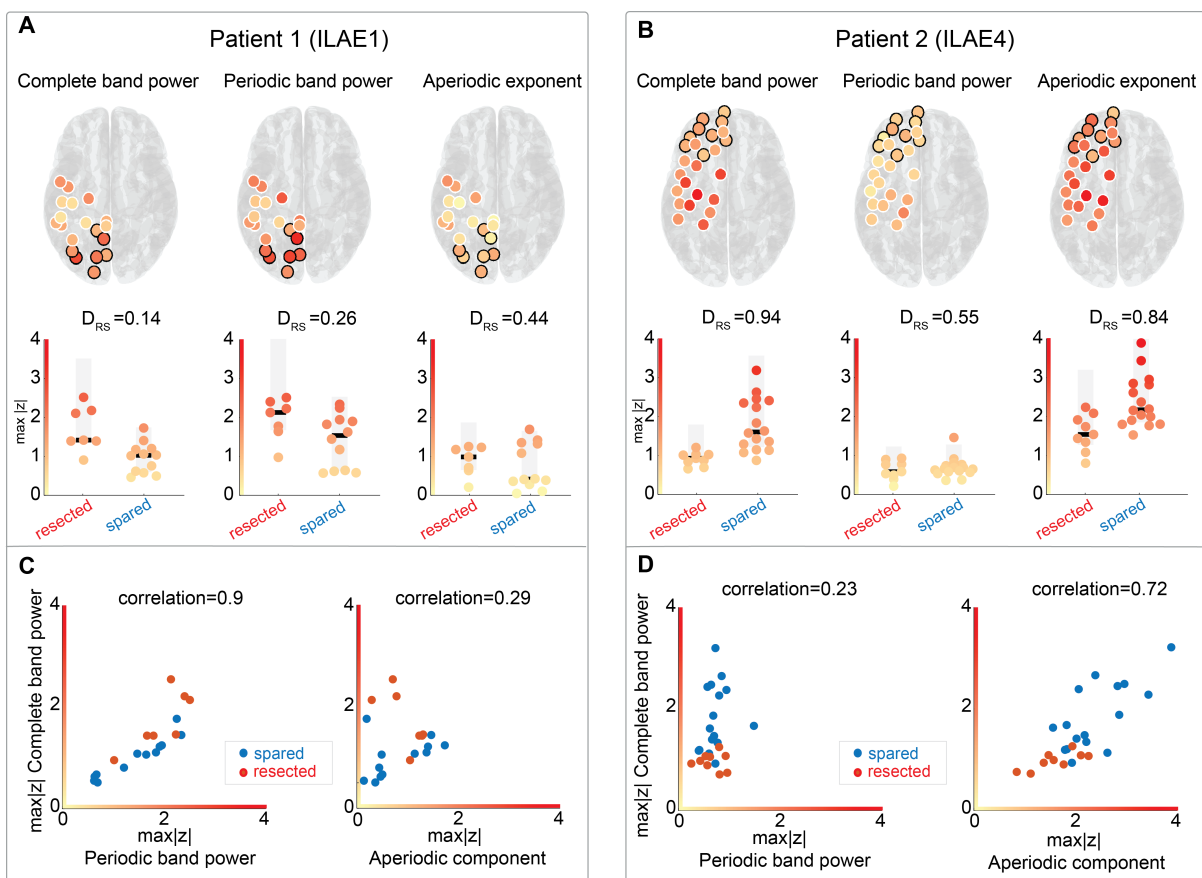


Figure 3: Different contributors to abnormality identified across relative complete band power, relative periodic band power and aperiodic exponent as a marker of resected and spared tissue in two example individual patients. Postoperative regions that were later surgically resected are circled in black. Non-resected regions are circled in white. (A) Patient 1 did not show signs of continued postoperative seizures (ILAE1), (B) Patient 2 did (ILAE4). The type of component that is most informative about the location of abnormality and outcome of patient appears to vary across patients. (C) ILAE1 patient, complete band power and periodic band power abnormalities correlate strongly, (D) ILAE4 patient show strong correlation between complete band power and aperiodic exponent abnormalities.

4.3 iEEG: Periodic and aperiodic features identify different parts of abnormality

The previous section suggests different factors can drive abnormalities in two patients, subsequently affecting D_{RS} . We next explored these factors across the larger cohort.

In the whole cohort, Figure 4A shows that abnormality estimated through the complete band power clearly separates good and bad outcome patients ($AUC=0.71$, $p<0.01$). However, neither periodic band power abnormalities (Fig. 4B) ($AUC=0.57$, $p=0.23$) nor aperiodic exponent abnormalities (Fig. 4C) ($AUC=0.56$, $p=0.27$) alone separated patient groups.

Figures 3 and 4ABC indicate that abnormalities may be driven by different components in different patients, in

different regions. We therefore next took an agnostic approach by computing the maximum abnormality, irrespective of the component used (periodic or aperiodic). In this approach we next selected the largest of the periodic and aperiodic abnormalities for each ROI (Fig. 4D). The D_{RS} values of these maximum abnormalities improved outcome classifications (AUC=0.64, p=0.05).

Complete band power D_{RS} values were only weakly correlated to the periodic band power D_{RS} values (Fig. S2.1A, Spearman's correlation=0.54) and aperiodic exponent D_{RS} values (Fig. S2.1B, Spearman's correlation=0.37). However, D_{RS} values computed from the maximum abnormalities were more strongly associated with the complete band power D_{RS} values (Fig. S2.1C, Spearman's correlation=0.71).

Thus, both periodic and aperiodic abnormalities were necessary to more accurately distinguish patient outcomes, with neither sufficient in isolation.

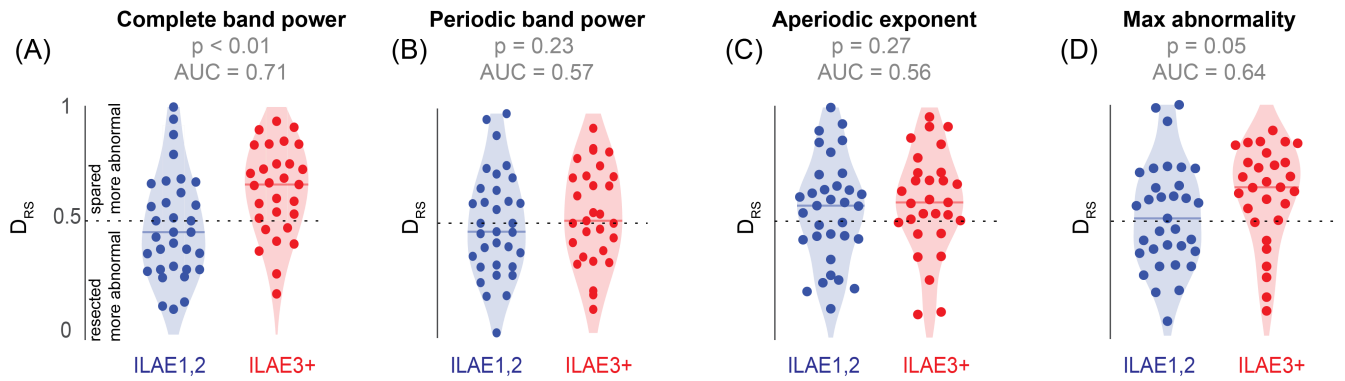


Figure 4: Both periodic and aperiodic abnormalities are necessary to distinguish patient outcomes, with neither sufficient in isolation (iEEG cohort). (A-D) Comparison of D_{RS} values between ILAE_{1,2} and ILAE₃₊ patients using (A) the complete band power abnormalities, (B) periodic band power abnormalities, (C) aperiodic exponent abnormalities, and (D) maximum abnormalities selected from periodic band power and aperiodic exponent abnormalities for each ROI. Each data point in the plot represents an individual patient, while the darker horizontal line denotes the median D_{RS} . AUCs were computed from the receiver operator characteristic curve (ROC) using D_{RS} as a binary classifier for surgical outcome.

4.4 MEG: Periodic and aperiodic features identify to different parts of abnormality

We repeated our analysis using resting-state MEG recordings by generating normative maps from 70 healthy controls and computing ROI abnormalities in 33 patients with refractory neocortical epilepsy. As in the iEEG analysis, neither periodic band power (Fig. 5B) (AUC=0.51, p=0.37) nor aperiodic exponent abnormalities (Fig. 5C) (AUC=0.59, p=0.14) distinguished patient outcomes well. However, the other two approaches (Fig. 5A,D) performed substantially better (complete band power AUC=0.69, p=0.03; max abnormality AUC=0.69, p=0.04).

Likewise, the complete band power and the periodic band power approaches was moderately correlated (Fig. S2.1D) (Spearman’s correlation=0.52), whereas the aperiodic approach only weakly correlated (Fig. S2.1E) (Spearman’s correlation=0.26). In contrast, the max abnormality approach exhibited a relatively strong correlation (Fig. S2.1F) (Spearman’s correlation=0.62).

These findings further suggest that neither periodic nor aperiodic abnormalities alone distinguish patient outcomes, but in combination they do. This agrees with the findings from iEEG data.

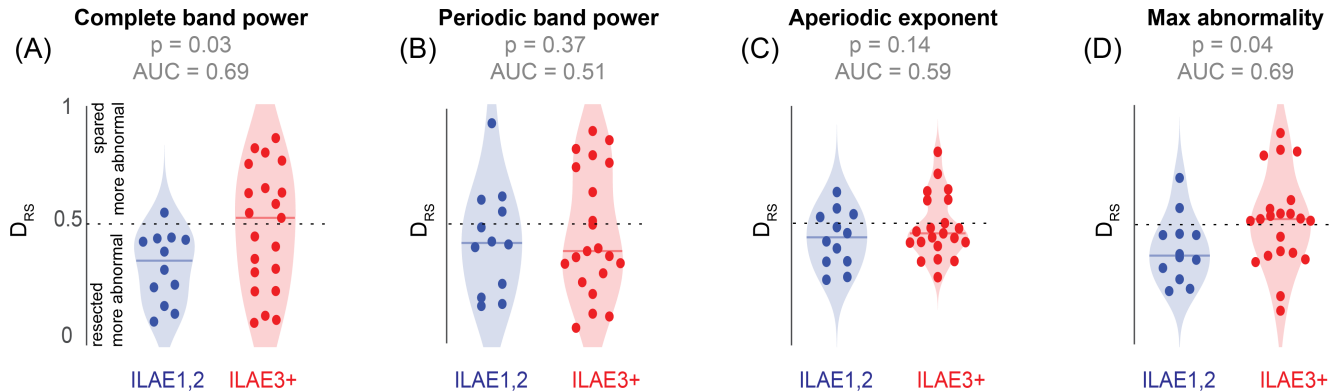


Figure 5: Both periodic and aperiodic abnormalities are necessary to distinguish patient outcomes, with neither sufficient in isolation (MEG cohort). (A) the complete band power abnormalities, (B) periodic band power abnormalities, (C) aperiodic exponent abnormalities, (D) maximum abnormalities selected from periodic band power and aperiodic exponent abnormalities for each ROI.

5 Discussion

We decomposed iEEG power spectra into periodic and aperiodic components to investigate the driving factors behind previously observed band power abnormalities. Using recordings from 234 subjects, we generated normative maps of complete band power, periodic band power, and the aperiodic exponent. We found that iEEG power spectra abnormalities of different patients were driven by distinct spectral features. Complete band power effectively distinguished between patients with good and bad outcomes, as previously reported (Bernabei et al., 2022; Owen et al., 2023; Taylor et al., 2022). However, neither periodic band power nor aperiodic exponent abnormalities alone provided the same discriminatory power, whilst their combination does. Repeating the same analysis on resting-state MEG recordings yielded consistent results with the iEEG cohort. Thus, both periodic and aperiodic abnormalities are important for abnormality mapping to predict patient outcomes.

While normative mapping approaches show promise to identify, classify and predict patient abnormalities and outcomes across different modalities (Bernabei et al., 2022; Owen et al., 2023; Rutherford et al., 2023; Sinha et al., 2017; Taylor et al., 2022; Wang et al., 2020), it is crucial to untangle the drivers of these abnormalities, which may help improve predictions and lead to improved mechanistic understanding of the underlying abnormality. Previous normative mapping approaches investigated how band power abnormality can be used to identify epileptogenic

areas and differentiate patient outcome based on resection (Bernabei et al., 2022; Owen et al., 2023; Taylor et al., 2022). Even if abnormality is identified through this method, the variety of underlying factors must be explored to gain a detailed picture about the nature of epileptogenic abnormality. Decomposing the power spectrum (Gerster et al., 2022; He, 2014; Miller et al., 2009; Muthukumaraswamy and Liley, 2018) provides a way to reveal the driving forces and determines the specific spectral components contributing to epileptogenic abnormalities. Toward this goal, we started with decomposing the power spectrum into periodic and aperiodic activity.

The source of aperiodic activity, following a $1/f$ power law, is highly debated (Buzsáki et al., 2012; Donoghue et al., 2022; He, 2014; Miller et al., 2009, 2014). The mechanisms behind this phenomenon may involve the combination of the nonlinear dynamics of neural networks, phase coherence-distance relationship between low and high frequency signals, low-pass filtering caused by the dendritic morphology of pyramidal cells, and the captive nature of the extracellular medium (Buzsáki et al., 2012; Miller et al., 2009, 2014). Other theories attribute the underlying mechanism to a near self-organised criticality (Banerjee et al., 2006; Miller et al., 2014; Stephani et al., 2020). In addition, Miller et al. (2009) proposed that the power spectral shape is due to the convolution of two functions, both exhibiting exponential decay. These functions represent the post-synaptic current and the membrane leak. Regardless of the exact source of the aperiodic activity, we hypothesized that besides that periodic activity, the contribution provided by the aperiodic component of the power spectrum is substantial.

We generated normative maps for iEEG aperiodic exponent values and found increased values, mainly in the temporal lobe. Although changes to the spatial patterns of aperiodic exponents during task or other activities have been shown in intracranial EEG (Podvalny et al., 2015; Sheehan et al., 2018), resting state normative maps have rarely been presented. Exploration of the spatial profile of this normative map requires further investigation. Although the focus of our study was on iEEG data, we also generated normative maps for MEG aperiodic exponent. These maps only partly follow the patterns that have been described previously (Donoghue et al., 2020a; Wilson et al., 2022). The differences, namely lower values in the occipital regions, may be caused by the fact that our MEG recordings were eyes closed while previous maps were based on eye open data sets. The periodic power distribution across the four frequency bands had consistent spatial patterns, mirroring those of complete band power. Similar patterns were found in previous studies (Bernabei et al., 2022; Frauscher et al., 2018; Groppe et al., 2013; Owen et al., 2023; Taylor et al., 2022). Namely, the anterior temporal and anterior frontal regions show the highest relative power in the delta frequency band, whereas the parietal and occipital regions demonstrate prominent relative power in the alpha frequency band. We found similar spatial patterns in MEG normative maps for both complete and periodic band power, concordant with previous studies (Donoghue et al., 2020a; Owen et al., 2023; Wilson et al., 2022).

We found that surgical sparing of cerebral tissue generating abnormalities in either periodic or aperiodic activity was associated with poor surgical outcomes, emphasizing the importance to analyze both types of abnormalities. Comparing abnormalities from periodic and aperiodic approaches and selecting the larger values across all ROIs,

improved outcome estimation. This suggests that the driving spectral component of abnormalities varies across regions and patients (see Fig. S3.1, S3.2, S3.3). Future studies could investigate whether periodic or aperiodic abnormalities depend on the location and nature of the underlying pathology. Both periodic band power and aperiodic exponents influence the changes in abnormality. While the aperiodic exponent in isolation cannot classify patient outcome in interictal data, other studies show that it is impactful for other aspects of epilepsy including seizure prediction and SOZ localization. van Heumen et al. (2021) and Yang et al. (2023) showed that the SOZ had a steeper aperiodic offset and exponent during seizures. Liu et al. (2023) pointed out that aperiodic features especially the exponent played a decisive role in classification of stages of epilepsy, while Kundu et al. (2023) showed that aperiodic exponent decreased over time following seizure freedom in a patient who went through multiple resection. Coa et al. (2022) also found that aperiodic parameters can be applied to analyze the efficacy of vagus nerve stimulation in patients with drug-resistant epilepsy. These findings have been supported by the idea that the excitation/inhibition (E/I) (im)balance can be estimated by the use of aperiodic exponent (Gao et al., 2017). Gao et al. (2017) pinpointed that changes in the balance of excitation and inhibition (E:I balance) are associated with alterations in the aperiodic exponent within a specific frequency range (30–70 Hz).

Previous studies indicated that interictal dynamics, besides focusing on narrow-band approaches, could offer valuable insights for the identification of abnormality (Chen et al., 2021; Höller et al., 2015). Interictal spikes, sharp waves, and high-frequency oscillations (HFOs) were proposed as putative biomarkers of epileptic activity. HFOs were proposed as a superior biomarker to identify epileptogenic tissue compared to spikes (Jacobs et al., 2008, 2010; van 't Klooster et al., 2017). HFOs were not as effective as spikes in guiding epilepsy surgery, overall and for temporal lobe epilepsy, and though there was a potential superiority of spikes over HFOs, HFO-guidance showed non-inferiority in the subgroup with extratemporal lobe epilepsy (Zweiphenning et al., 2022). Patients with positive outcome had a significantly higher percentage of HFO-generating areas removed compared to patients with a negative outcome (Jacobs et al., 2010). However, Roehri et al. (2018) concluded that HFOs were not superior biomarkers compared to interictal spikes and Gliske et al. (2018) found that HFO locations varied across different iEEG during sleep in most patients, spanning hours or days. While interictal spikes may manifest in the EEGs of patients, their surgical removal did not differentiate outcome groups (Taylor et al., 2022).

On the group level, neither periodic band power nor aperiodic exponent abnormalities alone distinguished patient outcome in iEEG or MEG cohorts. In both cases, we found that both periodic and aperiodic abnormalities are necessary to distinguish patient outcomes, with neither sufficient in isolation. In future studies, a quantitative multi-modal approach could be pursued to investigate abnormalities originating from periodic and aperiodic components. Possible approaches are directly comparing abnormalities across modalities or simulate multiple proposed surgeries and combining hypothetical D_{RS} values from multiple modalities to determine the optimal resection, as proposed by (Horsley et al., 2023).

Our work has limitations. We only explored the specparam solution for power spectrum decomposition, while

other approaches offer different mathematical solutions (Gerster et al., 2022; Wilson et al., 2022). Additionally, we limited our analysis to the power spectrum up to 30Hz to exclude potential issues with line noise and error-prone curve fitting at higher frequencies. Consequently, we excluded gamma band abnormalities from our analysis. While we used a straightforward method to measure the distinguishability between resected and spared tissue, there are other measures that solely consider the severity and size of abnormalities in resected tissue (Owen et al., 2023). Additionally, we only focused on localized abnormality while network based approaches may introduce more detailed insight into epileptogenic abnormality (Bernabei et al., 2022; Lagarde et al., 2018; Li et al., 2018; Shah et al., 2019; Sinha et al., 2021). Finally, we only considered one time period in our analysis, while it is important to understand the temporal aspects of these properties. However, Wang et al. (2023) showed that D_{RS} is a relatively robust metric across time, which suggests that our findings may also be temporally robust. Additionally, Wiesman et al. (2022) described the minimum amount of duration of recording necessary to obtain reliable estimates of both periodic and aperiodic components. While we used only 70 second epochs, they recommend longer time periods of MEG data (2-3 minutes, depending on the frequency band) to reliably estimate these features. Future studies are needed to investigate how different levels of signal to noise ratio influence these time intervals and if these recommendations also apply to iEEG data.

In conclusion, our study reveals that the type of spectral component providing the most information about abnormality location and patient outcome varies among patients. Consideration of both periodic and aperiodic abnormalities are necessary to distinguish spectral abnormalities. These findings further our goal to identify epileptogenic abnormalities and develop reliable methods to predict patient outcomes.

6 Acknowledgements

We thank members of the Computational Neurology, Neuroscience & Psychiatry Lab (www.cnnp-lab.com) for discussions on the analysis and manuscript; C.K. is supported by Epilepsy Research UK Foundation, P.N.T. and Y.W. are both supported by UKRI Future Leaders Fellowships (MR/T04294X/1, MR/V026569/1). JD, JdT are supported by the NIHR UCLH/UCL Biomedical Research Centre.

References

- Seppo P. Ahlfors, Jooman Han, John W. Belliveau, and Matti S. Hämäläinen. Sensitivity of meg and eeg to source orientation. *Brain Topography*, 23:227–232, 9 2010. ISSN 08960267. doi: 10.1007/s10548-010-0154-x.
- S. Baillet, J.C. Mosher, and R.M. Leahy. Electromagnetic brain mapping. *IEEE Signal Processing Magazine*, 18:14–30, 2001. ISSN 10535888. doi: 10.1109/79.962275.
- J Banerjee, M. K Verma, S Manna, and S Ghosh. Self-organised criticality and $1/f_i$ noise in single-channel current of voltage-dependent anion channel. *Europhysics Letters (EPL)*, 73:457–463, 2 2006. ISSN 0295-5075. doi: 10.1209/epl/i2005-10418-2.
- John M Bernabei, Nishant Sinha, T Campbell Arnold, Erin Conrad, Ian Ong, Akash R Pattnaik, Joel M Stein, Russell T Shinohara, Timothy H Lucas, Dani S Bassett, Kathryn A Davis, and Brian Litt. Normative intracranial eeg maps epileptogenic tissues in focal epilepsy. *Brain*, 145:1949–1961, 6 2022. ISSN 0006-8950. doi: 10.1093/brain/awab480.
- Richard F. Betzel, John D. Medaglia, Ari E. Kahn, Jonathan Soffer, Daniel R. Schonhaut, and Danielle S. Bassett. Structural, geometric and genetic factors predict interregional brain connectivity patterns probed by electrocorticography. *Nature Biomedical Engineering*, 3:902–916, 5 2019. ISSN 2157-846X. doi: 10.1038/s41551-019-0404-5.
- György Buzsáki, Costas A. Anastassiou, and Christof Koch. The origin of extracellular fields and currents-eeg, ecog, lfp and spikes. *Nature Reviews Neuroscience*, 13:407–420, 6 2012. ISSN 1471003X. doi: 10.1038/nrn3241.
- Zhuying Chen, Matias I. Maturana, Anthony N. Burkitt, Mark J. Cook, and David B. Grayden. High-frequency oscillations in epilepsy: What have we learned and what needs to be addressed. *Neurology*, 96:439–448, 3 2021. ISSN 1526632X. doi: 10.1212/WNL.0000000000011465.
- Roberta Coa, Simone Maurizio La Cava, Giulia Baldazzi, Lorenzo Polizzi, Giovanni Pinna, Carlo Conti, Giovanni Defazio, Danilo Pani, and Monica Puligheddu. Estimated eeg functional connectivity and aperiodic component induced by vagal nerve stimulation in patients with drug-resistant epilepsy. *Frontiers in Neurology*, 13, 11 2022. ISSN 1664-2295. doi: 10.3389/fneur.2022.1030118.
- Michele Angelo Colombo, Martino Napolitani, Melanie Boly, Olivia Gosseries, Silvia Casarotto, Mario Rosanova, Jean-Francois Brichant, Pierre Boveroux, Steffen Rex, Steven Laureys, Marcello Massimini, Arturo Chiaregato, and Simone Sarasso. The spectral exponent of the resting eeg indexes the presence of consciousness during unresponsiveness induced by propofol, xenon, and ketamine. *NeuroImage*, 189:631–644, 4 2019. ISSN 10538119. doi: 10.1016/j.neuroimage.2019.01.024.

- Jane de Tisi, Gail S Bell, Janet L Peacock, Andrew W McEvoy, William FJ Harkness, Josemir W Sander, and John S Duncan. The long-term outcome of adult epilepsy surgery, patterns of seizure remission, and relapse: a cohort study. *The Lancet*, 378:1388–1395, 10 2011. ISSN 01406736. doi: 10.1016/S0140-6736(11)60890-8.
- Thomas Donoghue, Julio Dominguez, and Bradley Voytek. Electrophysiological frequency band ratio measures conflate periodic and aperiodic neural activity. *eNeuro*, 7, 2020a. ISSN 23732822. doi: 10.1523/ENEURO.0192-20.2020.
- Thomas Donoghue, Matar Haller, Erik J. Peterson, Paroma Varma, Priyadarshini Sebastian, Richard Gao, Torben Noto, Antonio H. Lara, Joni D. Wallis, Robert T. Knight, Avgusta Shestyuk, and Bradley Voytek. Parameterizing neural power spectra into periodic and aperiodic components. *Nature Neuroscience*, 23:1655–1665, 12 2020b. ISSN 15461726. doi: 10.1038/s41593-020-00744-x.
- Thomas Donoghue, Natalie Schaworonkow, and Bradley Voytek. Methodological considerations for studying neural oscillations. *European Journal of Neuroscience*, 55:3502–3527, 6 2022. ISSN 14609568. doi: 10.1111/ejn.15361.
- Bruce Fischl. Freesurfer. *NeuroImage*, 62:774–781, 8 2012. ISSN 10538119. doi: 10.1016/j.neuroimage.2012.01.021.
- Birgit Frauscher, Nicolas von Ellenrieder, Rina Zelmann, Irena Doležalová, Lorella Minotti, André Olivier, Jeffery Hall, Dominique Hoffmann, Dang Khoa Nguyen, Philippe Kahane, François Dubeau, and Jean Gotman. Atlas of the normal intracranial electroencephalogram: neurophysiological awake activity in different cortical areas. *Brain*, 141:1130–1144, 4 2018. ISSN 0006-8950. doi: 10.1093/brain/awy035.
- Richard Gao, Erik J. Peterson, and Bradley Voytek. Inferring synaptic excitation/inhibition balance from field potentials. *NeuroImage*, 158:70–78, 9 2017. ISSN 10538119. doi: 10.1016/j.neuroimage.2017.06.078.
- Moritz Gerster, Gunnar Waterstraat, Vladimir Litvak, Klaus Lehnertz, Alfons Schnitzler, Esther Florin, Gabriel Curio, and Vadim Nikulin. Separating neural oscillations from aperiodic 1/f activity: Challenges and recommendations. *Neuroinformatics*, 20:991–1012, 10 2022. ISSN 15590089. doi: 10.1007/s12021-022-09581-8.
- Stephen V. Gliske, Zachary T. Irwin, Cynthia Chestek, Garnett L. Hegeman, Benjamin Brinkmann, Oren Sagher, Hugh J.L. Garton, Greg A. Worrell, and William C. Stacey. Variability in the location of high frequency oscillations during prolonged intracranial eeg recordings. *Nature Communications*, 9, 12 2018. ISSN 20411723. doi: 10.1038/s41467-018-04549-2.
- David M. Groppe, Stephan Bickel, Corey J. Keller, Sanjay K. Jain, Sean T. Hwang, Cynthia Harden, and Ashesh D. Mehta. Dominant frequencies of resting human brain activity as measured by the electrocorticogram. *NeuroImage*, 79:223–233, 10 2013. ISSN 10538119. doi: 10.1016/j.neuroimage.2013.04.044.

- Patric Hagmann, Leila Cammoun, Xavier Gigandet, Reto Meuli, Christopher J Honey, Van J Wedeen, and Olaf Sporns. Mapping the structural core of human cerebral cortex. *PLoS Biology*, 6:e159, 7 2008. ISSN 1545-7885. doi: 10.1371/journal.pbio.0060159.
- Biyu J. He. Scale-free brain activity: Past, present, and future. *Trends in Cognitive Sciences*, 18:480–487, 2014. ISSN 1879307X. doi: 10.1016/j.tics.2014.04.003.
- Jonathan J Horsley, Rhys H Thomas, Fahmida A Chowdhury, Beate Diehl, Andrew W McEvoy, Anna Miserocchi, Jane de Tisi, Sjoerd B Vos, Matthew C Walker, Gavin P Winston, John S Duncan, Yujiang Wang, and Peter N Taylor. Complementary structural and functional abnormalities to localise epileptogenic tissue. 4 2023.
- Yvonne Höller, Raoul Kutil, Lukas Klaffenböck, Aljoscha Thomschewski, Peter M. Höller, Arne C. Bathke, Julia Jacobs, Alexandra C. Taylor, Raffaele Nardone, and Eugen Trinka. High-frequency oscillations in epilepsy and surgical outcome. a meta-analysis. *Frontiers in Human Neuroscience*, 9, 10 2015. ISSN 16625161. doi: 10.3389/fnhum.2015.00574.
- Julia Jacobs, Pierre LeVan, Rahul Chander, Jeffery Hall, François Dubeau, and Jean Gotman. Interictal high-frequency oscillations (80-500 hz) are an indicator of seizure onset areas independent of spikes in the human epileptic brain. *Epilepsia*, 49:1893–1907, 11 2008. ISSN 00139580. doi: 10.1111/j.1528-1167.2008.01656.x.
- Julia Jacobs, Maeike Zijlmans, Rina Zelman, Claude Édouard Chatillon, Jeffrey Hall, André Olivier, François Dubeau, and Jean Gotman. High-frequency electroencephalographic oscillations correlate with outcome of epilepsy surgery. *Annals of Neurology*, 67:209–220, 2 2010. ISSN 03645134. doi: 10.1002/ana.21847.
- Mark Jenkinson, Christian F. Beckmann, Timothy E.J. Behrens, Mark W. Woolrich, and Stephen M. Smith. Fsl. *NeuroImage*, 62:782–790, 8 2012. ISSN 10538119. doi: 10.1016/j.neuroimage.2011.09.015.
- Bornali Kundu, Chantel M. Charlebois, Daria Nesterovich Anderson, Angela Peters, and John D. Rolston. Chronic intracranial recordings after resection for epilepsy reveal a ”running down” of epileptiform activity. *Epilepsia*, 64, 7 2023. ISSN 0013-9580. doi: 10.1111/epi.17645.
- Stanislas Lagarde, Nicolas Roehri, Isabelle Lambert, Agnes Trebuchon, Aileen McGonigal, Romain Carron, Didier Scavarda, Mathieu Milh, Francesca Pizzo, Bruno Colombet, et al. Interictal stereotactic-eeg functional connectivity in refractory focal epilepsies. *Brain*, 141(10):2966–2980, 2018.
- Janna D. Lendner, Randolph F. Helfrich, Bryce A. Mander, Luis Romundstad, Jack J. Lin, Matthew P. Walker, Pal G. Larsson, and Robert T. Knight. An electrophysiological marker of arousal level in humans. *eLife*, 9:1–29, 7 2020. ISSN 2050084X. doi: 10.7554/eLife.55092.

- Adam Li, Bhaskar Chennuri, Sandya Subramanian, Robert Yaffe, Steve Gliske, William Stacey, Robert Norton, Austin Jordan, Kareem A. Zaghloul, Sara K. Inati, Shubhi Agrawal, Jennifer J. Haagenzen, Jennifer Hopp, Chalita Atallah, Emily Johnson, Nathan Crone, William S. Anderson, Zach Fitzgerald, Juan Bulacio, John T. Gale, Sridevi V. Sarma, and Jorge Gonzalez-Martinez. Using network analysis to localize the epileptogenic zone from invasive eeg recordings in intractable focal epilepsy. *Network Neuroscience*, 2:218–240, 1 2018. ISSN 24721751. doi: 10.1162/netn.a.00043.
- Shan Liu, Jiang Wang, Shanshan Li, and Lihui Cai. Epileptic seizure detection and prediction in eegs using power spectra density parameterization. *IEEE Transactions on Neural Systems and Rehabilitation Engineering*, pages 1–1, 2023. ISSN 1534-4320. doi: 10.1109/TNSRE.2023.3317093.
- Kai J. Miller, Larry B. Sorensen, Jeffrey G. Ojemann, and Marcel den Nijs. Power-law scaling in the brain surface electric potential. *PLoS Computational Biology*, 5:e1000609, 12 2009. ISSN 1553-7358. doi: 10.1371/journal.pcbi.1000609.
- Kai J. Miller, Christopher J. Honey, Dora Hermes, Rajesh P.N. Rao, Marcel denNijs, and Jeffrey G. Ojemann. Broadband changes in the cortical surface potential track activation of functionally diverse neuronal populations. *NeuroImage*, 85:711–720, 1 2014. ISSN 10959572. doi: 10.1016/j.neuroimage.2013.08.070.
- Suresh D. Muthukumaraswamy and David TJ Liley. 1/f electrophysiological spectra in resting and drug-induced states can be explained by the dynamics of multiple oscillatory relaxation processes. *NeuroImage*, 179:582–595, 10 2018. ISSN 10959572. doi: 10.1016/j.neuroimage.2018.06.068.
- Brendan Ostlund, Thomas Donoghue, Berenice Anaya, Kelley E. Gunther, Sarah L. Karalunas, Bradley Voytek, and Koraly E. Pérez-Edgar. Spectral parameterization for studying neurodevelopment: How and why. *Developmental Cognitive Neuroscience*, 54, 4 2022. ISSN 18789307. doi: 10.1016/j.dcn.2022.101073.
- Thomas W. Owen, Gabrielle M. Schroeder, Vytene Janiukstyte, Gerard R. Hall, Andrew McEvoy, Anna Miserocchi, Jane de Tisi, John S. Duncan, Fergus Rugg-Gunn, Yujiang Wang, and Peter N. Taylor. γ abnormalities and mechanisms of surgical failure in neocortical epilepsy. *Epilepsia*, 64:692–704, 3 2023. ISSN 0013-9580. doi: 10.1111/epi.17503.
- Ella Podvalny, Niv Noy, Michal Harel, Stephan Bickel, Gal Chechik, Charles E Schroeder, Ashesh D Mehta, Misha Tsodyks, and Rafael Malach. A unifying principle underlying the extracellular field potential spectral responses in the human cortex. *J Neurophysiol*, 114:505–519, 2015. doi: 10.1152/jn.00943.2014.-Electrophysiological. URL www.jn.org.
- DARPA RAM. Restoring active memory: <https://memory.psych.upenn.edu/ram>. *DARPA dataset*, 2018.

- Sriharsha Ramaraju, Yujiang Wang, Nishant Sinha, Andrew W. McEvoy, Anna Miserocchi, Jane de Tisi, John S. Duncan, Fergus Rugg-Gunn, and Peter N. Taylor. Removal of interictal meg-derived network hubs is associated with postoperative seizure freedom. *Frontiers in Neurology*, 11, 9 2020. ISSN 1664-2295. doi: 10.3389/fneur.2020.563847.
- Nicolas Roehri, Francesca Pizzo, Stanislas Lagarde, Isabelle Lambert, Anca Nica, Aileen McGonigal, Bernard Giusiano, Fabrice Bartolomei, and Christian George Bénar. High-frequency oscillations are not better biomarkers of epileptogenic tissues than spikes. *Annals of Neurology*, 83:84–97, 1 2018. ISSN 15318249. doi: 10.1002/ana.25124.
- Saige Rutherford, Pieter Barkema, Ivy F Tso, Chandra Sripada, Christian F Beckmann, Henricus G Ruhe, and Andre F Marquand. Evidence for embracing normative modeling. 12:85082, 2023. doi: 10.7554/eLife.
- P. Shah, John M. Bernabei, Lohith G. Kini, A. Ashourvan, Jacqueline Boccanfuso, Ryan Archer, K. Oechsel, Sandhitsu R. Das, Joel M. Stein, Timothy H. Lucas, Danielle S. Bassett, Kathryn A. Davis, and B. Litt. High interictal connectivity within the resection zone is associated with favorable post-surgical outcomes in focal epilepsy patients. *NeuroImage: Clinical*, 23, 1 2019. ISSN 22131582. doi: 10.1016/j.nicl.2019.101908.
- Timothy C. Sheehan, Vishnu Sreekumar, Sara K. Inati, and Kareem A. Zaghloul. Signal complexity of human intracranial eeg tracks successful associative-memory formation across individuals. *Journal of Neuroscience*, 38: 1744–1755, 2 2018. ISSN 15292401. doi: 10.1523/JNEUROSCI.2389-17.2017.
- Nishant Sinha, Justin Dauwels, Marcus Kaiser, Sydney S. Cash, M. Brandon Westover, Yujiang Wang, and Peter N. Taylor. Predicting neurosurgical outcomes in focal epilepsy patients using computational modelling. *Brain*, 140: 319–332, 2 2017. ISSN 0006-8950. doi: 10.1093/brain/aww299.
- Nishant Sinha, Yujiang Wang, Nádia Moreira da Silva, Anna Miserocchi, Andrew W. McEvoy, Jane de Tisi, Sjoerd B. Vos, Gavin P. Winston, John S. Duncan, and Peter N. Taylor. Structural brain network abnormalities and the probability of seizure recurrence after epilepsy surgery. *Neurology*, 96:e758–e771, 2 2021. ISSN 1526632X. doi: 10.1212/WNL.0000000000011315.
- Tilman Stephani, Gunnar Waterstraat, Stefan Haufe, Gabriel Curio, Arno Villringer, and Vadim V. Nikulin. Temporal signatures of criticality in human cortical excitability as probed by early somatosensory responses. *Journal of Neuroscience*, 40:6572–6583, 8 2020. ISSN 15292401. doi: 10.1523/JNEUROSCI.0241-20.2020.
- François Tadel, Sylvain Baillet, John C. Mosher, Dimitrios Pantazis, and Richard M. Leahy. Brainstorm: A user-friendly application for meg/eeg analysis. *Computational Intelligence and Neuroscience*, 2011:1–13, 2011. ISSN 1687-5265. doi: 10.1155/2011/879716.

- Peter N. Taylor, Nishant Sinha, Yujiang Wang, Sjoerd B. Vos, Jane de Tisi, Anna Miserocchi, Andrew W. McEvoy, Gavin P. Winston, and John S. Duncan. The impact of epilepsy surgery on the structural connectome and its relation to outcome. *NeuroImage: Clinical*, 18:202–214, 2018. ISSN 22131582. doi: 10.1016/j.nicl.2018.01.028.
- Peter N. Taylor, Christoforos A. Papanavvas, Thomas W. Owen, Gabrielle M. Schroeder, Frances E. Hutchings, Fahmida A. Chowdhury, Beate Diehl, John S. Duncan, Andrew W. McEvoy, Anna Miserocchi, Jane De Tisi, Sjoerd B. Vos, Matthew C. Walker, and Yujiang Wang. Normative brain mapping of interictal intracranial eeg to localize epileptogenic tissue. *Brain*, 145:939–949, 3 2022. ISSN 14602156. doi: 10.1093/brain/awab380.
- Jeffrey R. Tenney, Hisako Fujiwara, and Douglas F. Rose. The value of source localization for clinical magnetoencephalography: Beyond the equivalent current dipole. *Journal of Clinical Neurophysiology*, 37:537–544, 11 2020. ISSN 0736-0258. doi: 10.1097/WNP.0000000000000487.
- Tam T. Tran, Camarin E. Rolle, Adam Gazzaley, and Bradley Voytek. Linked sources of neural noise contribute to age-related cognitive decline. *Journal of Cognitive Neuroscience*, 32:1813–1822, 9 2020. ISSN 0898-929X. doi: 10.1162/jocn.a.01584.
- José F. Téllez-Zenteno, Raj Dhar, and Samuel Wiebe. Long-term seizure outcomes following epilepsy surgery: A systematic review and meta-analysis. *Brain*, 128:1188–1198, 5 2005. ISSN 00068950. doi: 10.1093/brain/awh449.
- Saskia van Heumen, Jeremy T. Moreau, Elisabeth Simard-Tremblay, Steffen Albrecht, Roy W.R. Dudley, and Sylvain Baillet. Case report: Aperiodic fluctuations of neural activity in the ictal meg of a child with drug-resistant fronto-temporal epilepsy. *Frontiers in Human Neuroscience*, 15, 3 2021. ISSN 16625161. doi: 10.3389/fnhum.2021.646426.
- Maryse A. van 't Klooster, Nicole E.C. van Klink, Willemiek J.E.M. Zweiphenning, Frans S.S. Leijten, Rina Zelmann, Cyrille H. Ferrier, Peter C. van Rijen, Willem M. Otte, Kees P.J. Braun, Geertjan J.M. Huiskamp, and Maeike Zijlmans. Tailoring epilepsy surgery with fast ripples in the intraoperative electrocorticogram. *Annals of Neurology*, 81:664–676, 5 2017. ISSN 15318249. doi: 10.1002/ana.24928.
- Bradley Voytek and Robert T. Knight. Dynamic network communication as a unifying neural basis for cognition, development, aging, and disease. *Biological Psychiatry*, 77:1089–1097, 6 2015. ISSN 00063223. doi: 10.1016/j.biopsych.2015.04.016.
- Bradley Voytek, Mark A. Kramer, John Case, Kyle Q. Lepage, Zechari R. Tempesta, Robert T. Knight, and Adam Gazzaley. Age-related changes in 1/f neural electrophysiological noise. *Journal of Neuroscience*, 35:13257–13265, 9 2015. ISSN 15292401. doi: 10.1523/JNEUROSCI.2332-14.2015.

- Yujiang Wang, Nishant Sinha, Gabrielle M. Schroeder, Sriharsha Ramaraju, Andrew W. McEvoy, Anna Miserocchi, Jane Tisi, Fahmida A. Chowdhury, Beate Diehl, John S. Duncan, and Peter N. Taylor. Interictal intracranial electroencephalography for predicting surgical success: The importance of space and time. *Epilepsia*, 61:1417–1426, 7 2020. ISSN 0013-9580. doi: 10.1111/epi.16580.
- Yujiang Wang, Gabrielle M. Schroeder, Jonathan J. Horsley, Mariella Panagiotopoulou, Fahmida A. Chowdhury, Beate Diehl, John S. Duncan, Andrew W. McEvoy, Anna Miserocchi, Jane de Tisi, and Peter N. Taylor. Temporal stability of intracranial electroencephalographic abnormality maps for localizing epileptogenic tissue. *Epilepsia*, 6 2023. ISSN 0013-9580. doi: 10.1111/epi.17663.
- Samuel Wiebe, Warren T. Blume, John P. Girvin, and Michael Eliasziw. A randomized, controlled trial of surgery for temporal-lobe epilepsy. *New England Journal of Medicine*, 345:311–318, 8 2001. ISSN 0028-4793. doi: 10.1056/NEJM200108023450501.
- Alex I. Wiesman, Jason da Silva Castanheira, and Sylvain Baillet. Stability of spectral estimates in resting-state magnetoencephalography: Recommendations for minimal data duration with neuroanatomical specificity. *NeuroImage*, 247:118823, 2 2022. ISSN 10538119. doi: 10.1016/j.neuroimage.2021.118823.
- Luc Edward Wilson, Jason da Silva Castanheira, and Sylvain Baillet. Time-resolved parameterization of aperiodic and periodic brain activity. *eLife*, 11, 9 2022. ISSN 2050084X. doi: 10.7554/eLife.77348.
- Andrew I. Yang, Ashley L. B. Raghu, Faical Isbaine, Abdulrahman Alwaki, and Robert E. Gross. Sensing with deep brain stimulation device in epilepsy: Aperiodic changes in thalamic local field potential during seizures. *Epilepsia*, 9 2023. ISSN 0013-9580. doi: 10.1111/epi.17758.
- Willemieke Zweiphenning, Maryse A. van t. Klooster, Nicole E.C. van Klink, Frans S.S. Leijten, Cyrille H. Ferrier, Tineke Gebbink, Geertjan Huiskamp, Martine J.E. van Zandvoort, Monique M.J. van Schooneveld, M. Bourez, Sophie Goemans, Sven Straumann, Peter C. van Rijen, Peter H. Gosselaar, Pieter van Eijsden, Willem M. Otte, Eric van Diessen, Kees P.J. Braun, Maeike Zijlmans, Eltje M. Bloemen-Carlier, Veronika Cibulková, Renee de Munnink, Sandra van der Salm, Martinus J.C. Eijkemans, Janine M. Ophorst van Eck, Anouk Velders, Charlotte J.J. van Asch, Jack Zwemmer, Renate van Regteren-van Griethuysen, Henriette Smeding, Lydia van der Berg, Jeroen de Bresser, Gérard A.P. de Kort, and Jan Willem Dankbaar. Intraoperative electrocorticography using high-frequency oscillations or spikes to tailor epilepsy surgery in the netherlands (the hfo trial): a randomised, single-blind, adaptive non-inferiority trial. *The Lancet Neurology*, 21:982–993, 11 2022. ISSN 14744465. doi: 10.1016/S1474-4422(22)00311-8.

Supplementary

S1 Normative maps

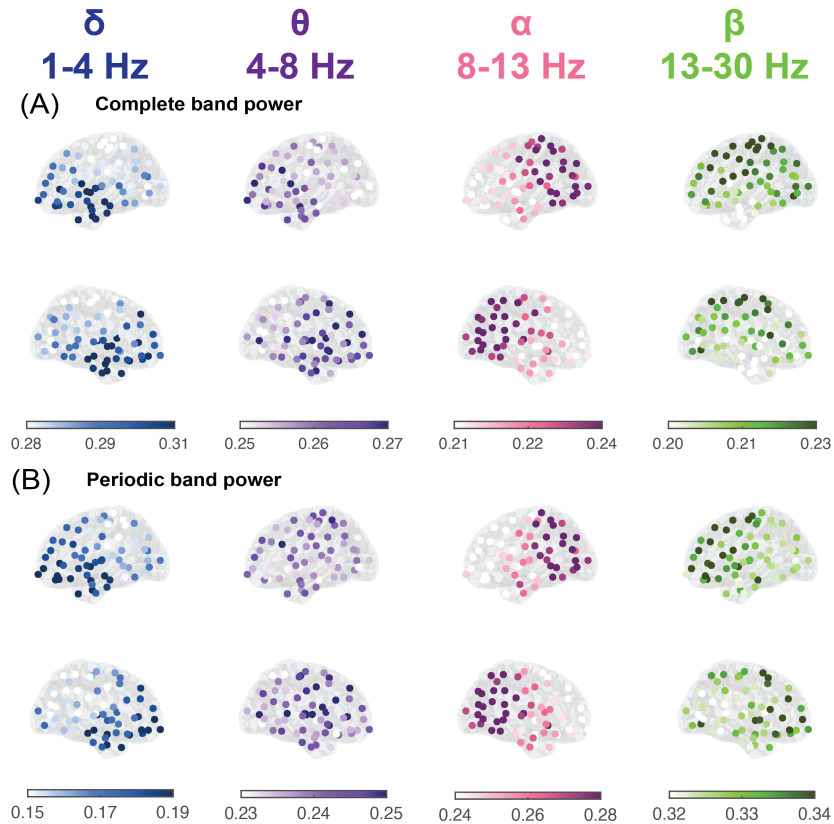


Figure S1.1: Side views of the normative maps generated based on (A) relative complete band power and (B) relative periodic band power

Figure S1.1 shows clear patterns as described in the main results section. The anterior temporal and frontal regions have the highest delta power, while the parietal and occipital regions show significant alpha power. Periodic band power reproduces the same spatial patterns observed in complete band power.

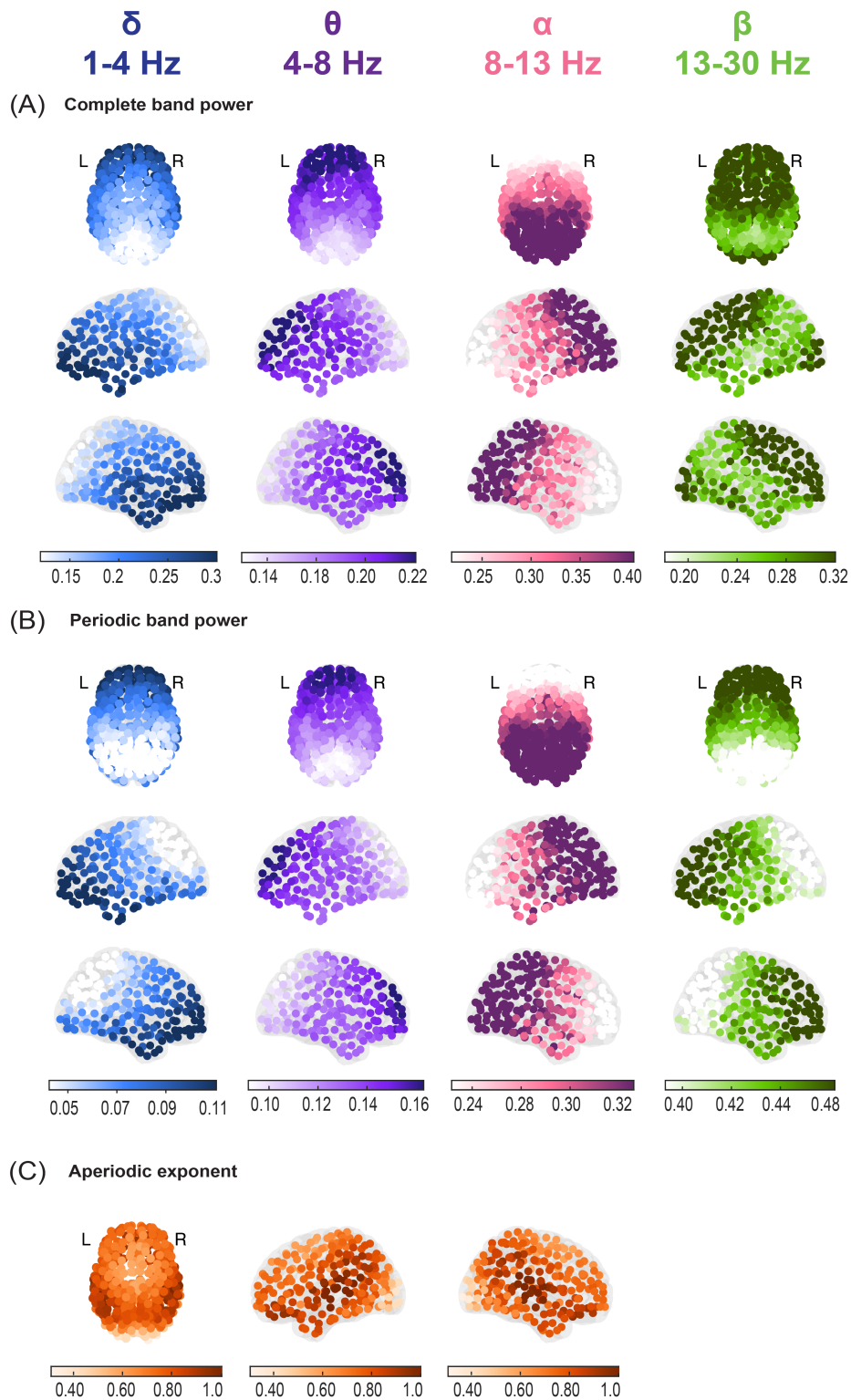


Figure S1.2: Normative maps of MEG relative complete band power, relative periodic band power, and aperiodic component. Spatial distribution of mean ROI values of, (A) relative complete band power, (B) relative periodic band power, and (C) aperiodic exponent

Figure S1.2 depicts similar patterns as the iEEG normative maps. Namely, the anterior temporal and frontal regions have the highest delta power, while the parietal and occipital regions show significant alpha power. Periodic

band power produces similar spatial patterns. In the aperiodic exponent maps, we found higher values in the posterior section of the temporal lobe and the parietal lobe. As mentioned in the main text, the MEG data set we used was eyes-closed recording, which may reduce exponent values in the occipital lobe.

S2 Correlation between abnormalities

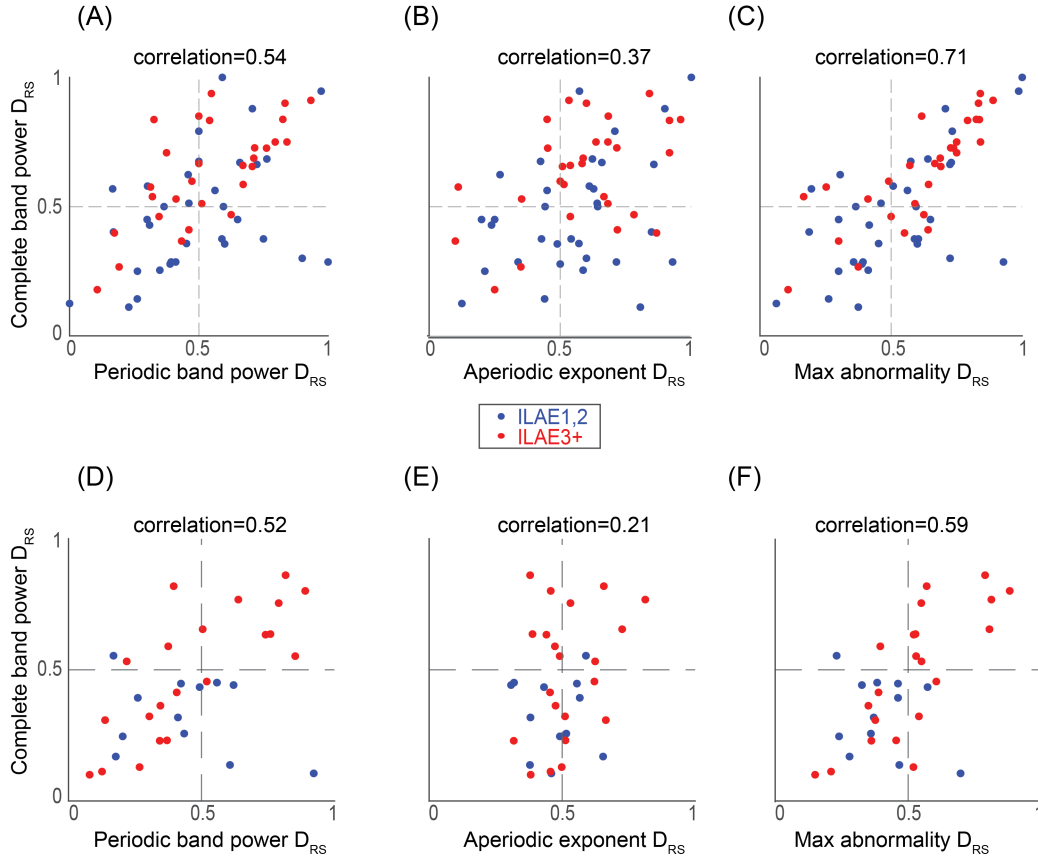


Figure S2.1: (A-C) Distribution of D_{RS} values obtained from the iEEG complete band power plotted against D_{RS} values based on abnormalities calculated from (A) periodic band power, (B) aperiodic exponent, and (C) maximum abnormalities selected from periodic band power and aperiodic exponent abnormalities for each ROI. Each data point in the plot represents an individual patient. Spearman’s ρ was used to quantify the correlation between each set of D_{RS} values. (D-F) Distribution of D_{RS} values obtained from the MEG complete band power plotted against D_{RS} values based on abnormalities calculated from (D) periodic band power, (E) aperiodic exponent, and (F) maximum abnormality based on periodic band power and aperiodic exponent.

Figure S2.1 shows that selecting the higher abnormality score across periodic band power and aperiodic component solutions yield D_{RS} scores that are closely correlated with the D_{RS} scores calculated from abnormalities based on the complete band power solution on the group level both in the iEEG and MEG cohorts.

S3 Proportion of features selected

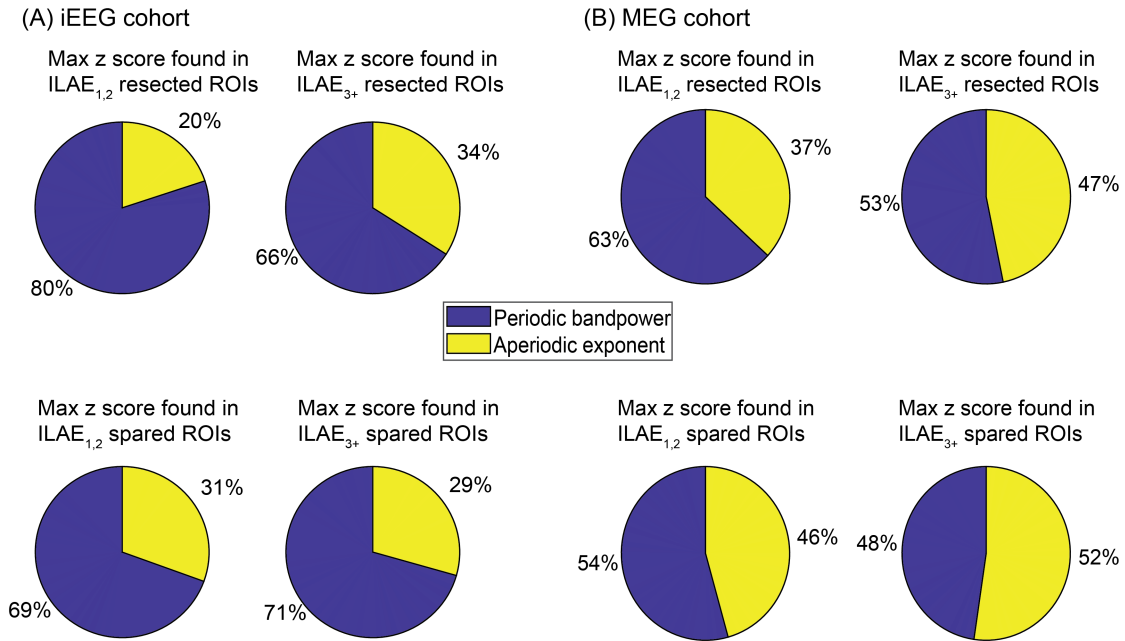


Figure S3.1: Proportion of maximum abnormality found from periodic band power and aperiodic exponent in (A) iEEG cohort and (B) MEG Cohort. .



Figure S3.2: Proportion of maximum abnormality found from each frequency band of the periodic band power and aperiodic exponent (iEEG cohort), separated by patient outcome.

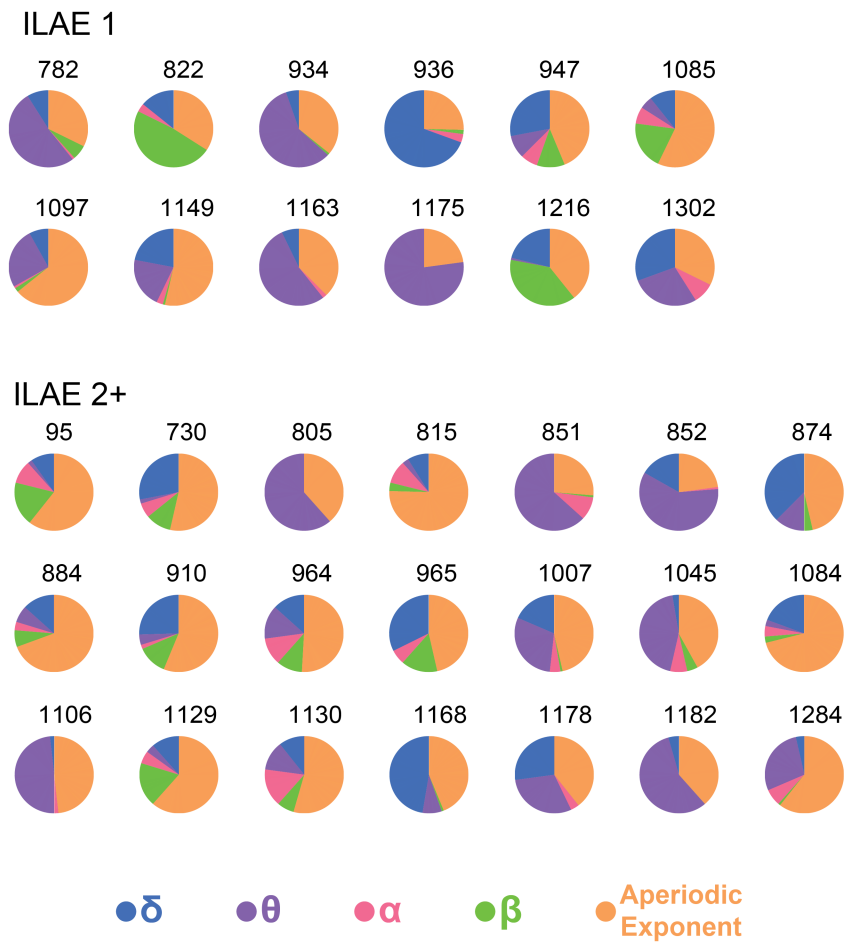


Figure S3.3: Proportion of maximum abnormality selected from each frequency band of the periodic band power and aperiodic exponent (MEG cohort), separated by patient outcome.

Figures S3.1, S3.2 and S3.3 indicate that abnormalities may be driven by different components (different frequency bands and aperiodic exponent) in different patients and in different regions. We therefore next computed the maximum abnormality, irrespective of the component used (periodic or aperiodic).

S4 Max abnormality selected in two example patients

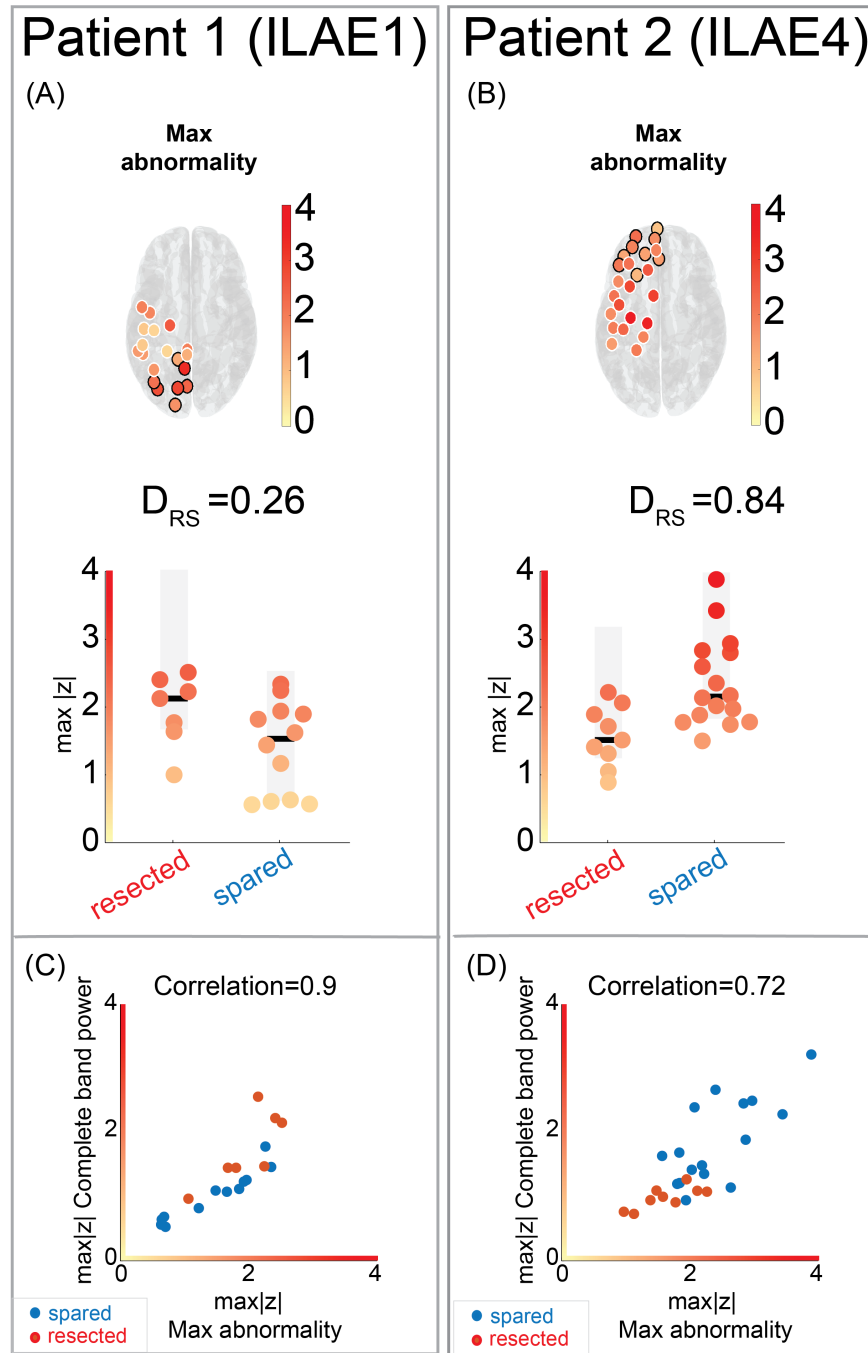


Figure S4.1: Max abnormality found in two example patients. Here we show the case when we select the higher abnormality score between periodic band power and aperiodic exponent for every ROI in a $ILAE_1$ (A) and an $ILAE_4$ (B) patient. Correlation calculated between the max abnormality scores and complete band power abnormality scores. In both patients (C-D), maximum abnormalities correlate high with complete band power abnormalities.

Fig. S4 demonstrates the high similarity between maximum abnormality values and complete band power abnormalities across all ROIs. This similarity is also reflected in the correlation between these measures in the two

example patients analyzed initially.